Photochemical & Photobiological Sciences
https://doi.org/10.1007/s43630-024-00626-2

ORIGINAL PAPERS

LED therapy modulates M1/M2 macrophage phenotypes and mitigates dystrophic features in treadmill-trained mdx mice

Valéria Andrade Pereira[1] · Heloina Nathalliê Mariano da Silva[1] · Evelyn Mendes Fernandes[1] · Elaine Minatel[1]

Received: 3 May 2024 / Accepted: 21 August 2024

Abstract

The *mdx* mouse phenotype, aggravated by chronic exercise on a treadmill, makes this murine model more reliable for the study of Duchenne muscular dystrophy (DMD) and allows the efficacy of therapeutic interventions to be evaluated. This study aims to investigate the effects of photobiomodulation by light-emitting diode (LED) therapy on functional, biochemical and morphological parameters in treadmill-trained adult *mdx* animals. M*dx* mice were trained for 30 min of treadmill running at a speed of 12 m/min, twice a week for 4 weeks. The LED therapy (850 nm) was applied twice a week to the quadriceps muscle throughout the treadmill running period. LED therapy improved behavioral activity (open field) and muscle function (grip strength and four limb hanging test). Functional benefits correlated with reduced muscle damage; a decrease in the inflammatory process; modulation of the regenerative muscular process and calcium signalling pathways; and a decrease in oxidative stress markers. The striking finding of this work is that LED therapy leads to a shift from the M1 to M2 macrophage phenotype in the treadmill-trained mdx mice, enhancing tissue repair and mitigating the dystrophic features. Our data also imply that the beneficial effects of LED therapy in the dystrophic muscle correlate with the interplay between calcium, oxidative stress and inflammation signalling pathways. Together, these results suggest that photobiomodulation could be a potential adjuvant therapy for dystrophinopathies.

Graphical abstract

Keywords Photobiomodation · *mdx* mice · Dystrophic muscle · Exercise · Oxidative stress · Inflammatory process · Calcium pathways

✉ Elaine Minatel
minatel@unicamp.br

[1] Departamento de Biologia Estrutural e Funcional, Instituto de Biologia, Universidade Estadual de Campinas (UNICAMP), Campinas, São Paulo 13083-970, Brazil

Published online: 04 September 2024

1 Introduction

Duchenne muscular dystrophy (DMD) is an X-linked disease caused by mutations in the gene that encodes the dystrophin protein, which is essential for muscle fiber integrity [1]. This disease is characterized by cycles of muscle degeneration, leading to progressive muscle weakness, loss of ambulation and premature death [2]. In addition, it is well established that a dysregulated inflammatory process plays a critical role in DMD progression [3] which is supported by the fact that corticosteroids are the standard therapy for dystrophic patients [4].

Macrophages are the predominant inflammatory cell type found in the skeletal muscles of dystrophic patients and the mdx mice, the pre-clinical model of DMD [5].

Although macrophages are normally essential for muscle regeneration, their dysregulated function promotes pathological muscle remodelling, such as the development of fibrosis [6]. The transition of macrophages from M1 (involved in pro-inflammatory responses) to M2 (related to anti-inflammatory action), usually seen in acute injury, is disrupted in the mdx mice by asynchronous bouts of muscle injury and regeneration [6]. In addition, it was recently demonstrated that dystrophic myofibers skew macrophages towards a pro-inflammatory phenotype, which in turn contributes to myofiber damage, increasing myofiber branching and fragility, thus exacerbating muscle damage and fibrosis [7]. Therefore, therapies that can modulate macrophage plasticity may constitute an important intervention to improve the dystrophic phenotype.

It was recently reported that photobiomodulation therapy (PBMT), a light-induced therapy applied by laser and/or light-emitting diodes (LED), modulates the inflammatory phase by decreasing M1 and increasing the M2 macrophages, thereby favoring muscle regeneration after an acute damage by crioinjury [8]. PBMT has been highlighted as a possible relevant therapy to improve the quality of life in dystrophic patients [9]. In dystrophic muscles from the experimental model of DMD, PBMT promoted improvements in regenerative capacity; reduction of inflammatory response and oxidative stress [10, 11]. Although preclinical animal experiments support PBMT as a therapeutic strategy for muscular dystrophies, the mechanisms behind the beneficial effects of this therapy in dystrophic muscles have not yet been fully elucidated. Thus, the aim of this study is to explore the effects of LED therapy in mdx mice with a phenotype aggravated by exercise, with a special focus on modulating macrophage phenotypes and their correlation with signalling pathways involved in the dystrophic muscle repair process. In addition, the results obtained will also be correlated with the functional data evaluated.

2 Material and methods

2.1 Animals and experimental design

All procedures with C57BL/10-Dmdmdx/PasUnib mice were approved by the Ethics Committee on the Use of Animals (CEUA) of the State University of Campinas (UNICAMP; #5982-1/2022) and following the guidelines of the Brazilian College for Animal Experimentation (COBEA). Mice chow and water were offered ad libitum and the animals were kept

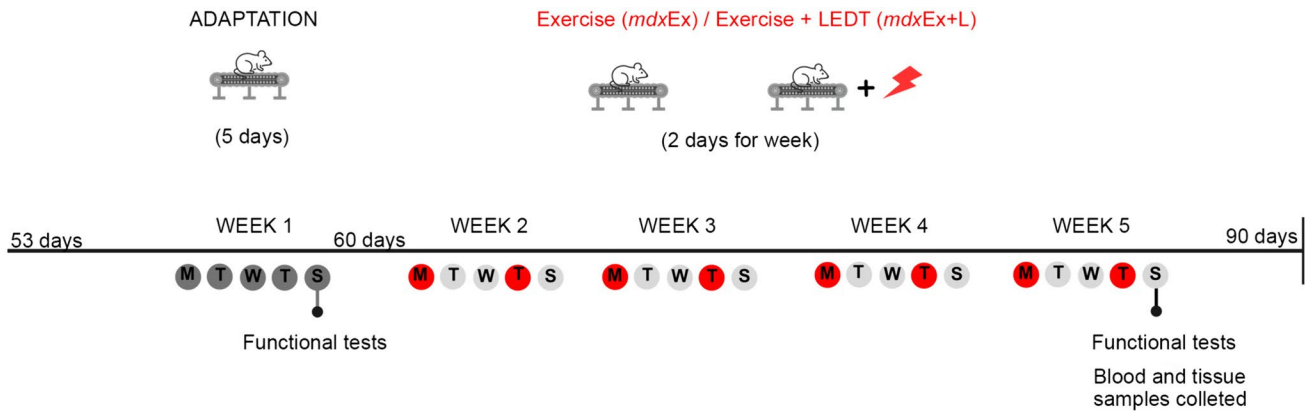

Fig. 1 Schematic showing the experimental timeline of treadmill exercise and LED therapy. Treadmill exercise and LED therapy was performed 2 times a week (red circles). Functional tests were performed after the last treadmill exercise in the adaptation period and endpoint (week 5) of the study. Blood for the analysis of plasma markers, and muscles for histopathology and Western blot were collected at the endpoint (week 5)

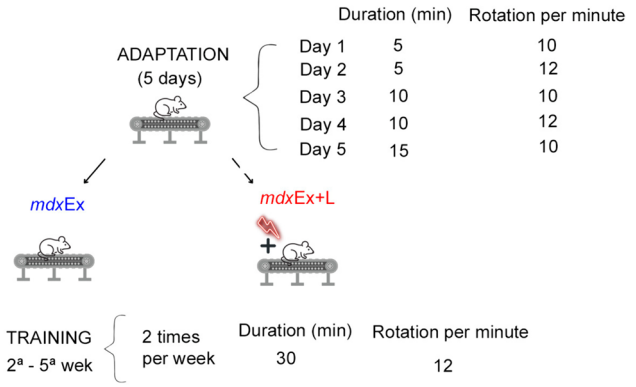

Fig. 2 Treadmill exercise parameters in adaptation and training period

in a temperature-controlled room (25 °C ± 0.5) and relative humidity (55 ± 1) with 12-h light/ dark cycles. The protocol of the experiment is shown in Fig. 1. Male m*dx* mice (53 days old) were randomly assigned into three groups: *mdxSed*, sedentary controls; *mdx*Ex, exercise-trained animals; and *mdx*Ex + L, exercise-trained animals submitted to LED therapy.

2.2 Treadmill exercise and LED therapy

The treadmill exercise protocol was performed using the TREAT-NMD [12], protocols for exercise in *mdx* mice and also based on a previous work of our research group [13]. The training protocol was divided into two phases consisting of adaptation and exercise (Fig. 2). After the first week of adaptation, the protocol consisted of a treadmill exercise regime of 30 min treadmill running at a speed of 12 m/min twice per week for 4 weeks (keeping a constant interval of 2–3 days between each trial).

LED therapy protocol was based on a previous work of a research group [14], the PBMT took place transcutaneously at one point in the center of the quadriceps femoris muscular venter, at a distance of 3 cm (without contact). Both hind limbs were irradiated and the application lasted 10 s per session with fixed parameters as described in Table 1. LED therapy sham had no energy and no power applied over the quadriceps femoris muscular venter. The irradiation occurred twice per week for four consecutive weeks.

Twenty-four hours after the last training session and LED therapy, the animals were euthanized using a mixture of ketamine hydrochloride (130 mg/kg; Franco tar, Virbac, Fort Worth, TX, USA) and xylazine hydrochloride (6.8 mg/kg, 2% Virbaxil; Virbac), and the blood samples were collected by cardiac puncture and quadriceps femoris muscle was removed.

Table 1 LED therapy parameters

LED therapy parameters	
Output power (mW)	300
Spot size (cm^2)	0.32
Power density (mW/cm^2)	937
Energy per point (J)	3
Energy density (J/cm^2)	9.37
Time per point(s)	10
Format	Circular
Operating mode	Continuous
Number and frequency of treatment sessions	8, 2 times a week
Application technique	Transcutaneous in the middle of the belly quadriceps femoris muscle

2.3 Functional tests: grip strength, hanging tests and open field

Functional tests were performed before the start of treadmill exercise and LED therapy and twenty-four hours after the last training session and LED irradiation.

2.3.1 Grip strength (*n* = 28 per group)

A grip strength meter (New Primer, Sao Paulo, Brazil) was used to measure the forelimb muscle strength, following the protocol based on previous studies of our research group [14]. This protocol consists of collecting three measurements from each animal and normalize the absolute strength (average of five measurements) to body weight.

2.3.2 Hanging test (*n* = 7 per group)

The hanging test is applied to evaluate muscle function, neuromuscular impairment, and motor coordination [15, 16]. The protocol used in this study was based on the Treat-NMD protocol DMD_M.2.1.005. The mice were placed on a metal grid measuring 35 cm in length and 22 cm in width, with 22 metal wires spaced 6 mm apart. Then the grid was turned upside down, suspended 35 cm above a padded cage to ensure a soft landing after the fall. The measurement of the retention impulse result was obtained by the suspension time multiplied by body weight. The test was performed in 3 attempts, with 15 min of rest between each attempt. A stopwatch was used to record the suspension time of each animal.

2.3.3 Open field (*n* = 7 per group)

To apply this test, a white chamber measuring 45 cm × 60 cm × 40 cm wall height, with 12 squares

(15 cm × 15 cm each) applied to the floor of the chamber, was used. The protocol used in this study was based on a previous study [17]. After 1 h of adaptation in the testing room, the mice were placed in a corner of the chamber and left free to explore. Horizontal movements, such as crossing each square with all paws, were counted for 6 min.

2.4 Blood and quadriceps femoris samples for muscle fiber degeneration analysis (*n* = 7 per group)

For biochemical assessment of muscle fiber degeneration, the creatine kinase (CK) assay was evaluated in the blood and quadriceps femoris samples. The protocol used in this study was based on a previous study [14]. The CK assay was carried out using a commercially available kit (CK Cinetico Crystal, BioClin, Ireland) and a BioTek Spectrophotometer (BioTek Instruments Inc., Winooski, VT, USA). Values are reported as international units per liter.

2.5 Histopathological analysis (*n* = 7 per group)

Histomorphology protocols were based on previous studies [13, 14]. For all morphological analysis, serial cryosections (8 µm) of quadriceps femoris muscle were used and observed under a light microscope or fluorescent microscope.

2.5.1 Muscle fiber damage

For morphological visualization and quantification of muscle fiber damage in the quadriceps femoris muscle, cryosections were incubated with fluorescently labeled immunoglobulin (Ig) G. Briefly, muscle cryosections (8 µm thick) were preincubated for 30 min with 5% bovine serum albumin (BSA) in phosphate-buffered saline (PBS), followed by a 1 h incubation with IgG fluorescein isothiocyanate conjugate antibody (anti-mouse; Sigma-Aldrich, St Louis, MO, USA). The number of IgG-labeled muscle fibers was quantified manually using the Image-Pro Plus 6.0 software (Media Cybernetics, Silver Spring, MD, United States) and expressed as a percentage of the total number of muscle fibers counted in each cross-section (5 cross-sectional areas per muscle).

2.5.2 Fibrotic area

Cryosection of quadriceps muscles was stained with Masson's trichrome for quantitative observation of fibrosis and the fibrosis area and total muscle area were manually delimited and calculated using the Image-Pro Plus 6.0 software (Media Cybernetics, Silver Spring, MD, United States). Fibrosis area was expressed as a percentage of the total area.

2.5.3 Regenerated muscle fibers

Cryosections of quadriceps femoris muscle were stained with hematoxylin and eosin (HE) and the number of regenerated muscle fibers (with central nuclei) and normal (with peripheral nuclei) was quantified manually using the Image-Pro Plus 6.0 software (Media Cybernetics, Silver Spring, MD, United States). The number of regenerated muscle fibers was expressed as a percentage of the total number of fibers (normal and regenerated). In addition, about 100 normal and regenerated muscle fibers were evaluated for minimum Feret's diameter.

2.5.4 Inflammatory area

Cryosections of quadriceps femoris muscle were stained with HE and the inflammatory area and total muscle area were manually delimited and calculated using the Image-Pro Plus 6.0 software (Media Cybernetics, Silver Spring, MD, United States). Inflammatory area was expressed as a percentage of the total area.

2.5.5 Macrophage infiltration

Cryosections of quadriceps femoris muscle were incubated with F4/80 antibody and the macrophage infiltration area and total muscle area were manually delimited and calculated using the Image-Pro Plus 6.0 software (Media Cybernetics, Silver Spring, MD, United States). Macrophage infiltration area was expressed as a percentage of the total area.

2.5.6 Oxidative stress: autofluorescent granules of lipofuscin and reactive DHE area

The number of autofluorescent granules of lipofuscin and the intensity of reactive Dihydroethidium (DHE) was quantified using the Image-Pro Plus 6.0 software (Media Cybernetics, Silver Spring, MD, United States).

For quantification of the number of autofluorescent granules of lipofuscin, muscle samples were analyzed using serial cryosections unfixed (8 µm) of the quadriceps femoris muscle. Quantification was performed in a fluorescent inverted microscope (Nikon, Eclipse TS100/TS100F) and the total number of lipofuscin granules was determined in relation to the total area of the cut by their thickness (number of lipofucin/μm^3).

For quantification of the intensity of reactive DHE, serial quadriceps femoris muscle cryosections (8 µm) were incubated with 5 µl DHE (λ_{ex} 358 nm; λ_{em} 461 nm). DHE staining presents a bright red emission in fluorescence microscopy. The intensity of reactive DHE by muscle area was quantified using a fluorescent inverted microscope (Nikon, Eclipse TS100) by measuring pixels in a specific range

(70 ± 255 wavelength). The equipment was adjusted to eliminate interference from background fluorescence.

2.6 Protein quantification by Western Blot (*n* = 7 per group)

Western blot protocol was based on previous studies (13, 14). Briefly, muscle samples were homogenized using homogenizer Polytron PTA 20S (model PT 10/35; Kinematica Ag). Muscle sample detritus was removed by centrifugation and the cleared lysate was subjected to SDS-Page gel electrophoresis. The Bradford method was used to determine the total protein content. Total protein from muscle sample lysate (30 µg) was stacked on 12% sodium dodecyl sulfate (SDS)-polyacrylamide gels. The proteins were transferred from gels to nitrocellulose membranes by electrophoresis. A blocking buffer was used in all membranes for 2 h at room temperature. Membranes were incubated with appropriated primary antibodies overnight at 4 °C with gentle shaking. The following primary antibodies were used for Western blotting: MyoD (rabbit polyclonal IgG; M-318/Santa-Cruz); Myogenin (mouse monoclonal IgG_1 κ; F5D/Santa-Cruz); MyHC-slow (monoclonal anti-myosin (skeletal, slow); mouse IgG1; M8421/Sigma-Aldrich); MyHC-fast (monoclonal anti-myosin (skeletal, fast); mouse IGg1; M4276/Sigma-Aldrich); Anti-Mannose (mouse monoclonal mannose receptor antibody; mouse IgG1; ab8918/Abcam); Anti-Nitric Oxide Synthase (monoclonal anti-nitric oxide synthase; inducible antibody produced in mouse; N9657/Sigma-Aldrich); NFkB (NFkB p65 (pSer53); polyclonal IgG; AHP1342/Bio-RAD); 4-HNE (goat anti-4-hydroxynonenal; polyclonal IgG; AHP1251/Bio-RAD); SERCA1 (monoclonal; rabbit IgG; D54G12/Cell Signaling Technology); Calsequestrin (mouse monoclonal; mouse / IgG2b; VIIID12/ThermoFisher Scientific); and β-actin (anti-β-actin antibody; mouse monoclonal; A1978/Sigma-Aldrich). The following peroxidase-conjugated secondary antibodies were used for Western blotting: mouse (mouse IgG; 1:2500, 04-18-06, KPL, USA); goat (goat IgG; 1:1000, 14-13-06, KPL, USA); and rabbit (rabbit IgG; 1:2500, 04-15-06, KPL, USA). Membranes were incubated with peroxidase-conjugated secondary antibodies for 2 h at room temperature and then washed 3 times for 10 min each with Tris-buffered saline containing 0.1% Tween® 20 detergent (TBST). Anti-β-Actin antibody was used as a control protein loading. All membranes were revealed using the Clarity Western ECL Substrate (Bio-Rad). Gene Tools from Syngene were used for bands intensity quantification.

2.7 Statistical analysis

All data are expressed as mean ± standard deviation (SD). Statistical analysis for direct comparison between means of groups was performed by ANOVA, followed by the Tukey test used for multiple statistical comparisons between groups. $p \leq 0.05$ was considered statistically significant. We have used the GraphPad Prims8 software package (GraphPad Software, CA, USA).

3 Results

3.1 LED therapy effects on body weight and functional performance

All experimental groups experienced weight gain during the experimental period: by 10.10% in the mdxSed mice group, 9.74% in the mdxEx group and 12.81% in the mdxEx + L mice group (Fig. 3A).

The animals in the mdxEx group showed reduced performance in all muscle functional tests (Grip strength, Hanging test and Open Field) after the trial period compared to before the trial period (Fig. 3B–D). In contrast, LED therapy improved functional performance in the mdxEx + L group. These animals demonstrated improvement in all three muscle functional tests evaluated after the trial period (Fig. 3B–D). Specifically, the mdxEx + L group showed significantly higher grip strength (by 42.72%), better performance in hanging test (by 96.94%), and improved open field results (by 46.66%) compared to the mdxEx group.

3.2 LED therapy effects on the muscular degeneration process

The animals in the mdxEx group showed significantly higher levels in the biochemical assessment of muscle fiber degeneration (Table 2). Specifically, these animals exhibited significantly elevated CK serum levels (by 77.72%) compared to the mdx sedentary group (Table 2). In contrast, the mdxEx + L group demonstrated significantly lower levels of muscle fiber degeneration, as indicated by significantly reduced CK serum levels (by 98.60%) and significantly higher CK levels in the quadriceps femoris muscle (by 64.91%) compared to the mdxEx group (Table 2). Additionally, the mdxEx + L group showed significantly lower levels in the morphological evaluation of muscle fiber degeneration, evidenced by reduced intracellular fiber staining with IgG antibody in the quadriceps femoris muscles (by 63.35%) compared to the mdxEx group (Fig. 4A, B).

The fibrotic area in the quadriceps femoris muscles of the experimental groups was also evaluated (Fig. 4C, D). The fibrotic area was significantly higher in the quadriceps femoris muscle of the mdxEx group (by 67.75%) compared to the mdxS group (Fig. 4D). In contrast, the mdxEx + L group exhibited a significantly lower fibrotic area in the

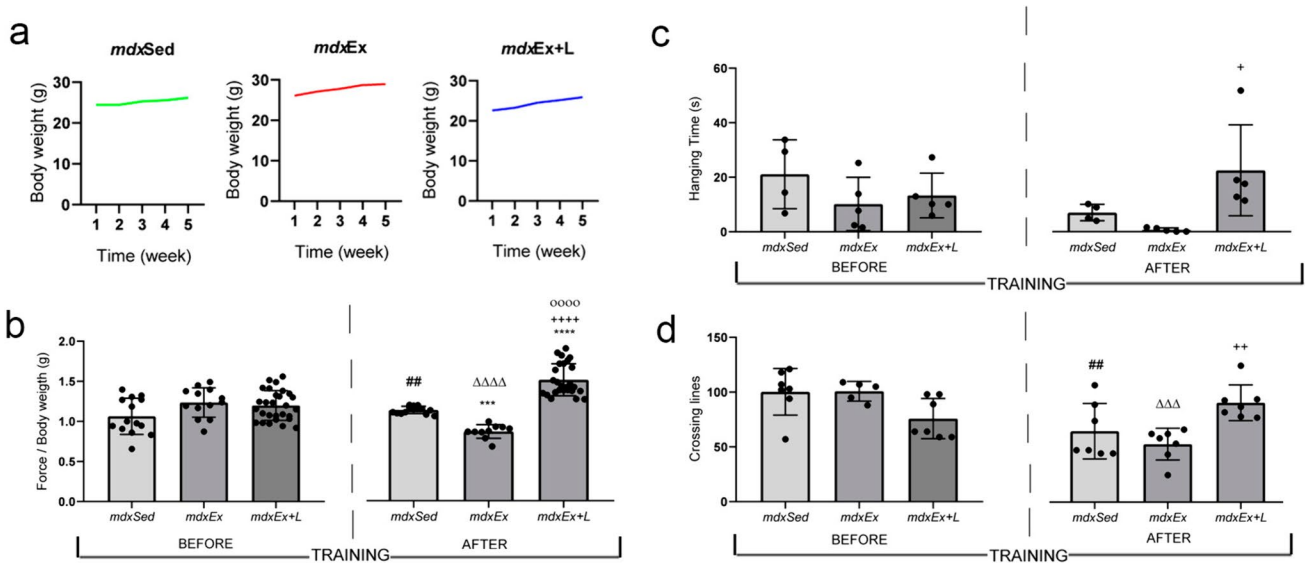

Fig. 3 **a** Body weight (g) was measured weekly during the experimental period. **b** Forelimb muscle strength was assessed by taking measurements of force, before and after the experimental period, normalized by body weight (g/g). **c** Four limb hanging test and **d** Open field test was performed before and after the experimental period. Experimental groups: mdx sedentary controls (mdxSed); mdx exercise-trained (mdxEx); and mdx exercise-trained submitted to LED therapy (mdxEx + L). All data are expressed by mean ± SD. $^{\#\#}P < 0.01$ versus mdxSed before training; $^{\Delta}P < 0.00001$ versus mdxEx before training; $^{\circ\circ\circ\circ}P < 0.00001$ versus mdxEx + L before training; $^{***}P < 0.001$ versus mdxSed after training; $^{****}P < 0.00001$ versus mdxSed after training; $^{++++}P < 0.00001$ versus mdxEx after training. One-way ANOVA followed by Tukey post-test was used for statistical analysis

Table 2 Creatine kinase levels

	Blood creatine kinase (U/L)	Muscle creatine kinase (U/L)
*mdx*Sed	2214 ± 374,2	2469 ± 151,4
*mdx*Ex	9935 ± 1064****	1239 ± 573,2
*mdx*Ex + L	$139.5 \pm 20.58^{++++}$	$3531 \pm 1245^{++}$

Values are expressed as mean ± standard deviation (SD). Experimental groups: mdx sedentary controls (mdxSed); mdx exercise-trained (mdxEx); and mdx exercise-trained submitted to LED therapy (mdxEx + L). All data are expressed by mean ± SD. $^{****}P < 0.00001$ versus mdxSed; $^{++}P < 0.01$ versus mdxEx; and $^{++++}P < 0.00001$ versus mdxEx. One-way ANOVA followed by Tukey post-test was used for statistical analysis

quadriceps femoris muscles (by 75.67%) compared to the mdxEx group (Fig. 4D).

3.3 LED therapy effects on regenerative muscular process and on myogenic regulatory factors

The mdxEx + L group demonstrated an improvement in the regenerative muscle process, as indicated by significantly fewer in fibers with central nuclei (by 19.58%) and significantly more fibers with peripheral nuclei (by 41.02%) in the quadriceps femoris muscle compared to the mdxEx group (Fig. 5A, B). Additionally, a significantly larger regenerated muscle fiber diameter was observed in the mdxEx + L group (by 26.37%) compared to the mdxEx group (Fig. 5C). Concomitantly, a higher quadriceps femoris muscle weight was also observed in the mdxEx + L group (by 35.77%) compared to the mdxEx group (Fig. 5D).

Regarding the myogenic regulatory factors, the mdxEx group showed significantly higher Myo-D levels (by 81.95%) and significantly lower myogenin levels (by 65.36%) in the quadriceps femoris muscle, compared to the mdxSed group (Fig. 6A–C). In contrast, the mdxEx + L animals showed significantly lower Myo-D levels (by 76.62%) and significantly higher myogenin levels (by 66.36%) in the quadriceps femoris muscle compared to the mdxEx group (Fig. 6A–C).

With respect to myosin heavy chains levels, the mdxEx + L animals exhibited significantly higher MyHC-slow levels (by 48.04%) and a significant decrease in MyHC-fast levels (by 50.27%) in the quadriceps femoris muscle compared to the mdxEx group (Fig. 6D, E).

3.4 LED therapy effects on inflammatory response

The mdxEx group exhibited a significantly larger inflammatory area (by 39.85%) in the quadriceps femoris muscle, compared to the mdxSed group (Fig. 7A, B). In contrast, the mdxEx + L group showed a significantly reduced inflammatory area (by 96.24%) in the quadriceps femoris muscle compared to the mdxEx group (Fig. 7A, B).

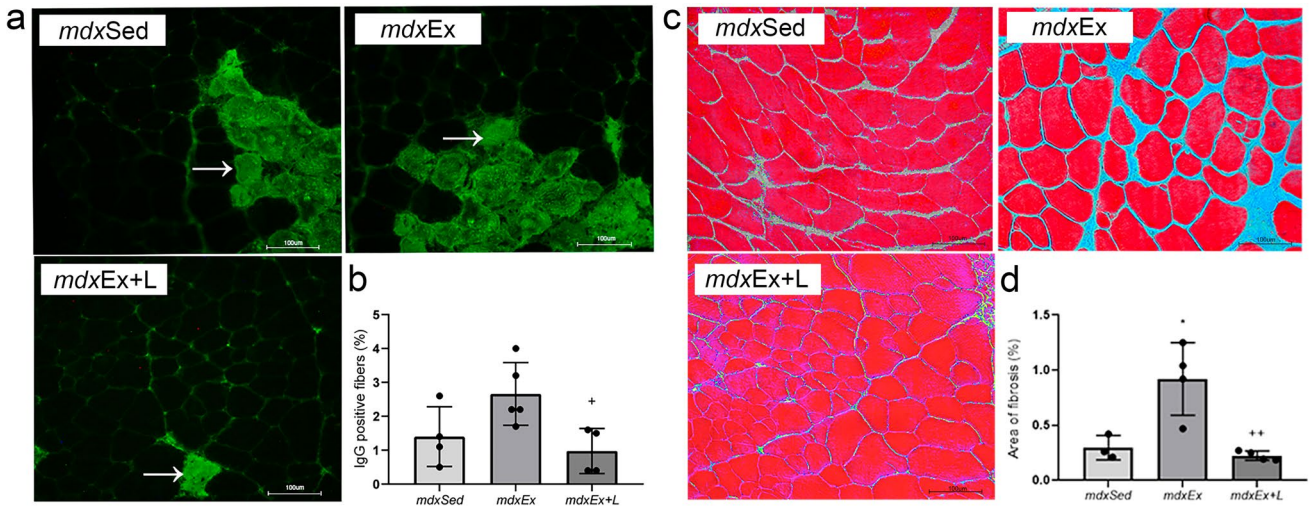

Fig. 4 Cross sections of quadriceps femoris muscle showing: **a** IgG staining (white arrows) and **c** fibrosis area (blue color) in mdx sedentary controls (mdxSed); mdx exercise-trained (mdxEx); and mdx exercise-trained submitted to LED therapy (mdxEx + L). Scale bar 100 µm, × 20. The graphs show: **b** the IgG staining (%) and **d** the percentage of fibrosis area in all experimental groups. All data are expressed by mean ± SD. $^{*}P < 0.05$ versus mdxSed; $^{+}P < 0.05$; versus mdxEx; and $^{++}P < 0.01$ versus mdxEx. One-way ANOVA followed by Tukey post test was used for statistical analysis

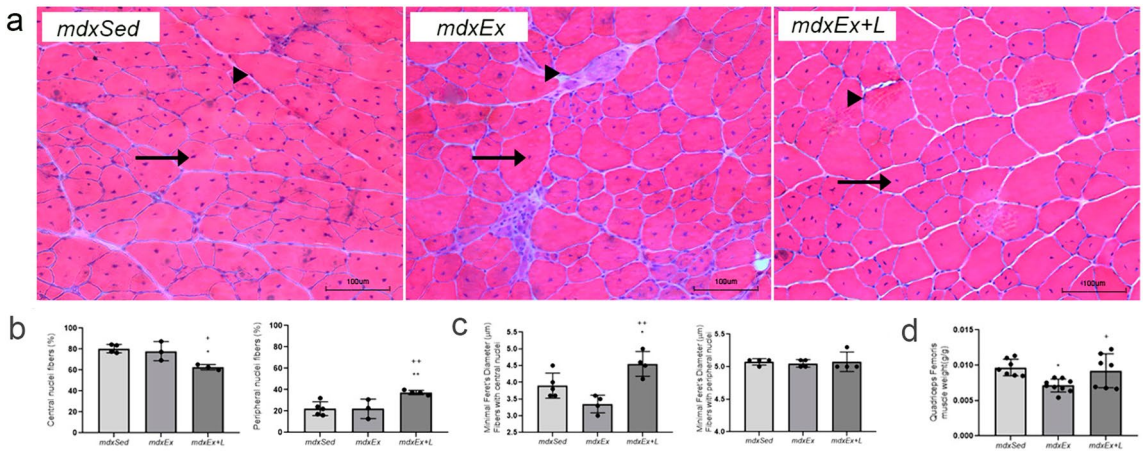

Fig. 5 Cross sections of quadriceps femoris muscle showing: **a** fibers with central nuclei (black arrows) and with peripheral nuclei (black arrowheads) in mdx sedentary controls (mdxSed); mdx exercise-trained (mdxEx); and mdx exercise-trained submitted to LED therapy (mdxEx + L). Scale bar 100 µm, × 20. The graphs show: **b** the percentage of fibers with central nuclei fibers and fibers with peripheral nuclei; **c** the minimal Feret'sdiameter (µm) of fibers with central nuclei and fibers with peripheral nuclei; and **d** the quadriceps femoris muscle weight in all experimental groups. All data are expressed by mean ± SD. $^{*}P < 0.05$ versus mdxSed; $^{**}P < 0.01$ versus mdxSed; $^{+}P < 0.05$; versus mdxEx; and $^{++}P < 0.01$ versus mdxEx. One-way ANOVA followed by Tukey post test was used for statistical analysis

In addition, the mdxEx group exhibited significantly higher macrophage infiltration area (by 56.63%) in the quadriceps femoris muscle compared to the mdxSed group (Fig. 7C, D). In contrast, the mdxEx + L group showed significantly lower macrophage infiltration area (by 81.80%) in the quadriceps femoris muscle compared to the mdxEx group (Fig. 7C, D).

Regarding the macrophage analysis, the mdxEx + L animals showed significantly lower M1 levels (by 47.57%) and significantly higher M2 levels (by 44.76%) in the quadriceps femoris muscle compared to the mdxEx group (Fig. 8A–C).

Additionally, the mdxEx + L group exhibits significantly lower NF-κB levels (by 70.81%) in the quadriceps femoris muscle compared to the mdxEx group (Fig. 8A, D).

3.5 LED therapy effects on oxidative stress

The mdxEx group showed increased oxidative stress in the quadriceps femoris muscle, as indicated by significantly

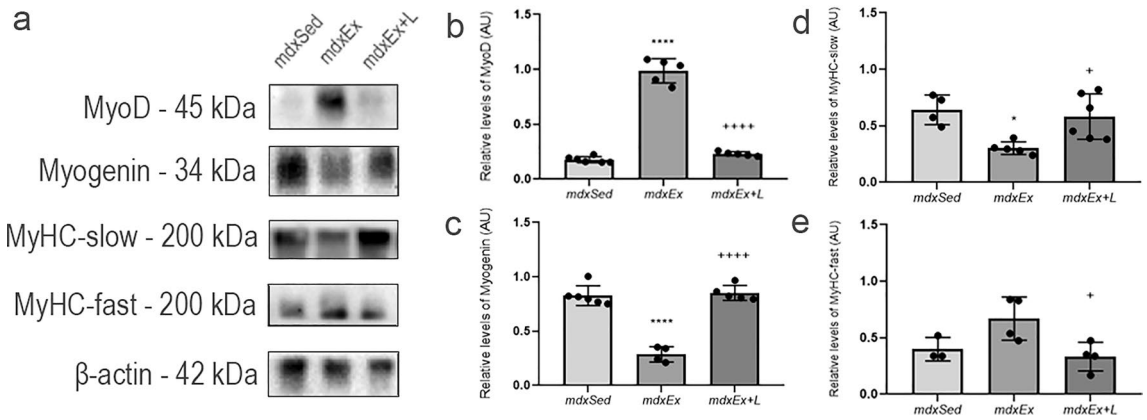

Fig. 6 Western blotting data: **a** MyoD; myogenin; MCH-slow; and MHC-fast in mdx sedentary controls (mdxSed); mdx exercise-trained (mdxEx); and mdx exercise-trained submitted to LED therapy (mdxEx + L). The graphs show: **b** MyoD; **c** myogenin; **d** MCH-slow; and **e** MHC-fast in all experimental groups. Loading control: β-actin. All data are expressed by mean ± SD. $^{*}P < 0.05$ versus mdxSed; $^{****}P < 0.00001$ versus mdxSed; $^{+}P < 0.05$; versus mdxEx; and $^{++++}P < 0.00001$ versus mdxEx. One-way ANOVA followed by Tukey post-test was used for statistical analysis

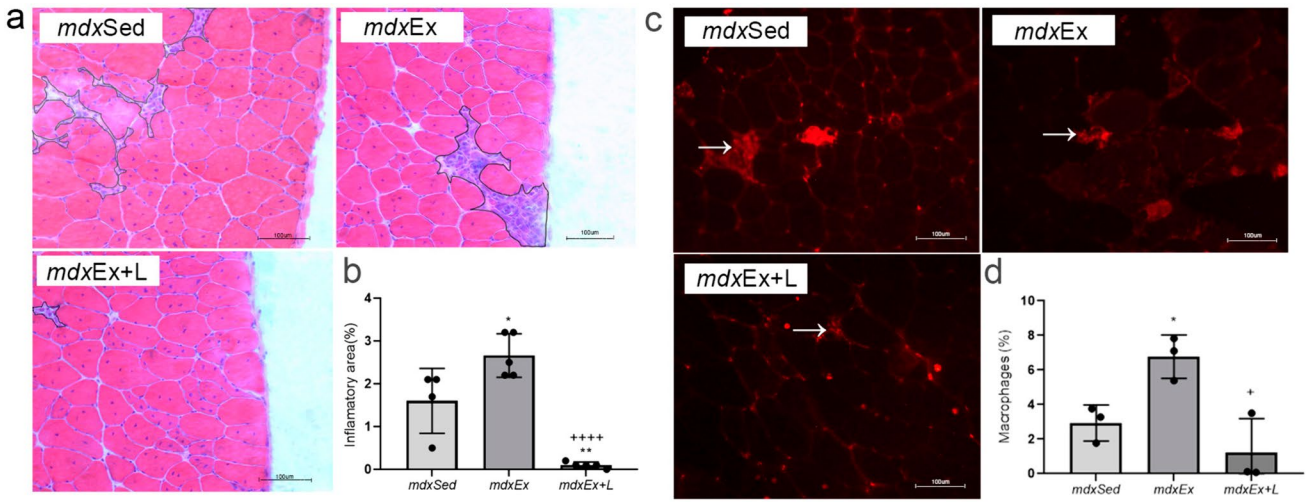

Fig. 7 Cross sections of quadriceps femoris muscle showing: **a** inflammatory area (outline) and **c** macrophage infiltration (white arrows) in mdx sedentary controls (mdxSed); mdx exercise-trained (mdxEx); and mdx exercise-trained submitted to LED therapy (mdxEx + L). Scale bar 100 µm, × 20. The graphs show: **b** the percentage of inflammatory area and **d** the percentage of macrophage infiltration in all experimental groups. All data are expressed by mean ± SD. $^{*}P < 0.05$ versus mdxSed; $^{**}P < 0.01$ versus mdxSed; $^{+}P < 0.05$; versus mdxEx; and $^{++++}P < 0.00001$ versus mdxEx. One-way ANOVA followed by Tukey post-test was used for statistical analysis

higher levels of reactive DHE area; autofluorescent lipofuscin granules; and 4-HNE protein adduct (by 7.18%; 33.01% and 42.64%, respectively) compared to the mdxSed group (Fig. 9A–F). In contrast, the mdxEx + L animals exhibited significantly lower levels of DHE area; autofluorescent lipofuscin granules; and 4-HNE protein adduct (by 51.38%; 42.89% and 66.45%, respectively) compared to the mdxEx group (Fig. 9A–F).

3.6 LED therapy effects on calcium-binding protein

The mdxEx + L animals showed significantly higher SERCA 1 levels (by 31.63%) and calsequestrin levels (by 40.91%) in the quadriceps femoris muscle compared to the mdxEx group (Fig. 10A, B).

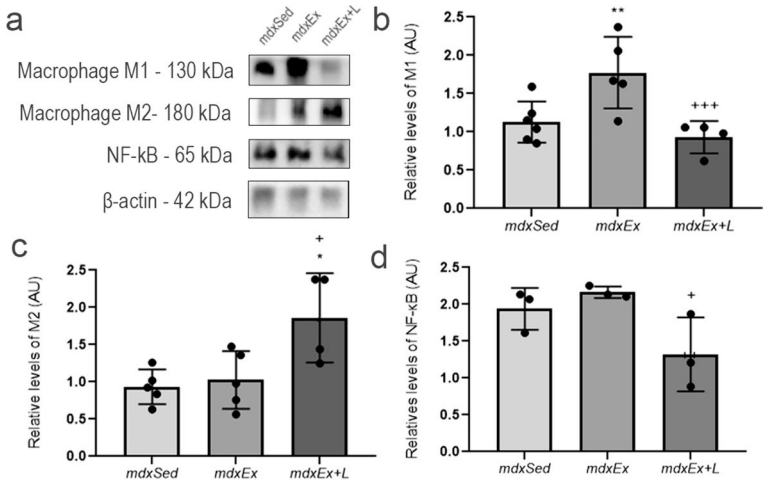

Fig. 8 Western blotting data: **a** macrophage M1; macrophage M2; and NF-κB in mdx sedentary controls (mdxSed); mdx exercise-trained (mdxEx); and mdx exercise-trained submitted to LED therapy (mdxEx + L). The graphs show: **b** M1; **c** M2; and **d** NF-κB in all experimental groups. Loading control: β-actin. All data are expressed by mean ± SD. $^{*}P < 0.05$ versus mdxSed; $^{**}P < 0.01$ versus mdxSed; $^{+}P < 0.05$; versus mdxEx; and $^{+++}P < 0.0001$ versus mdxEx. One-way ANOVA followed by Tukey post-test was used for statistical analysis

4 Discussion

In this study, treadmill-trained mdx mice were chosen as a model for preclinical DMD research to evaluate the effects of LED therapy on dystrophic muscle. Treadmill-trained mdx mice exhibit a worsening of the dystrophic phenotype, characterized by functional impairment and increased muscle damage, making this preclinical model closer to human dystrophy and allowing potential therapeutic

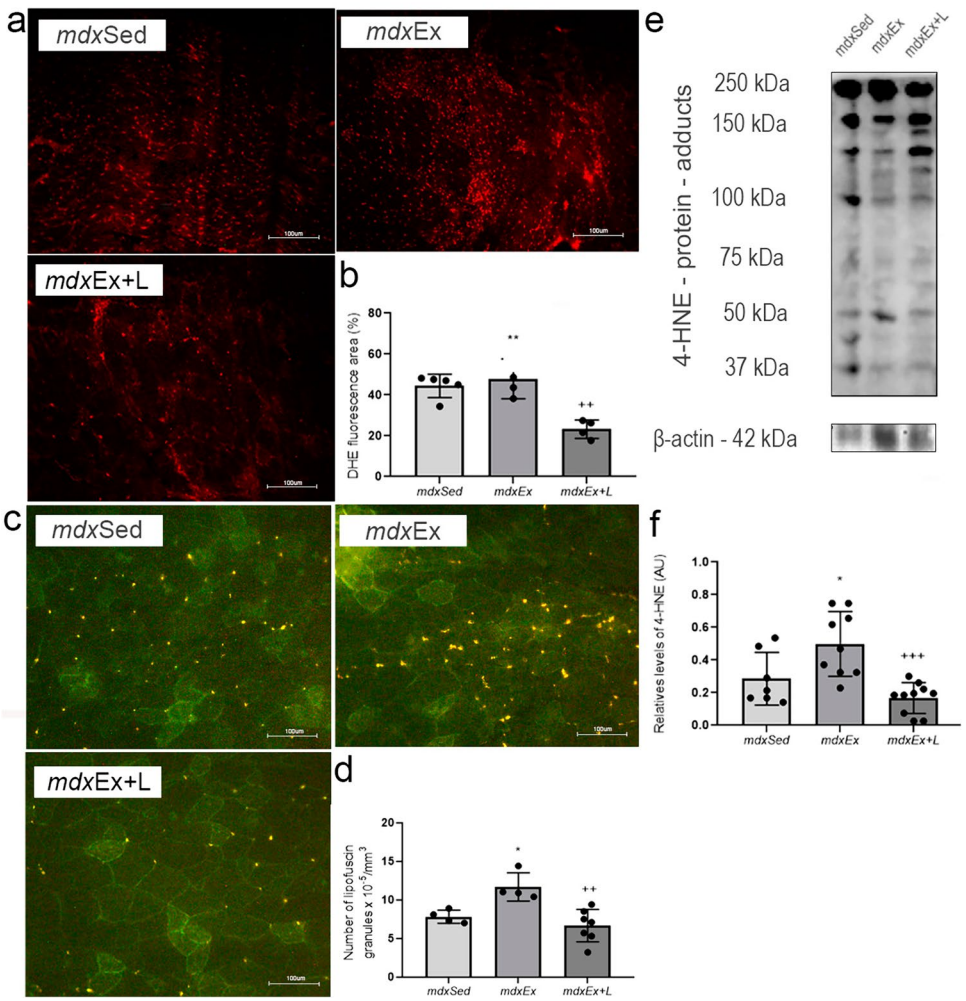

Fig. 9 Cross sections of quadriceps femoris muscle showing: **a** dihydroethidium (DHE) fluorescence (red) and **c** autofluorescent lipofuscin granules (brownish granule) in mdx sedentary controls (mdxSed); mdx exercise-trained (mdxEx); and mdx exercise-trained submitted to LED therapy (mdxEx + L). Scale bar 100 µm, × 20. The graphs show: **b** the percentage of DHE staining area and **d** the number of lipofuscin granules $\times 10^{-4}/mm^3$ in all experimental groups. Western blotting data (**e**) and graph (**f**): 4-hydroxynonenal (4-HNE)-protein adducts in all experimental groups. Loading control: β-actin. All data are expressed by mean ± SD. $^{*}P < 0.05$ versus mdxSed; $^{**}P < 0.01$ versus mdxSed; $^{++}P < 0.01$ versus mdxEx; and $^{+++}P < 0.0001$ versus mdxEx. One-way ANOVA followed by Tukey post-test was used for statistical analysis

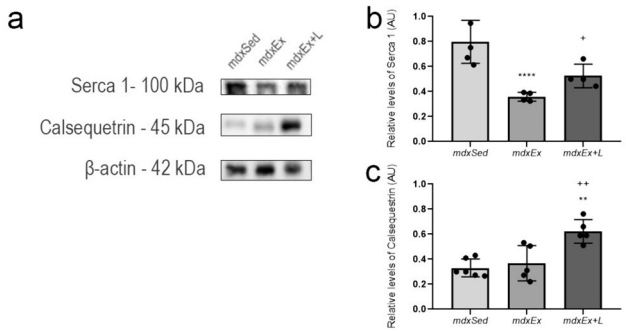

Fig. 10 Western blotting data: **a** Serca 1; calsequestrin in mdx sedentary controls (mdxSed); mdx exercise-trained (mdxEx); and mdx exercise-trained submitted to LED therapy (mdxEx + L). The graphs show: **b** Serca 1; and **c** calsequestrin in all experimental groups. Loading control: β-actin. All data are expressed by mean ± SD. $^{**}P < 0.01$ versus mdxSed; $^{****}P < 0.00001$ versus mdxSed; $^{+}P < 0.05$; versus mdxEx; and $^{++}P < 0.01$ versus mdxEx. One-way ANOVA followed by Tukey post-test was used for statistical analysis

interventions to be more rigorously evaluated in in vivo studies [13, 18].

One of the most important findings of the present work is that LED therapy modulates the inflammatory process in treadmill-trained mdx mice by increasing the M2 and decreasing the M1 macrophage phenotypes. In addition to this result, a significant reduction in the inflammatory and macrophage infiltration areas and in nuclear factor kappa B (NF-κB) levels, was observed. NF-κB is an important prototypic signalling cascade that drives classical (M1) activation of macrophages [19]. Previous studies have linked the down-regulation of NF-κB to a decrease in the M1 macrophage phenotype under different experimental conditions [20, 21]. These studies corroborate our findings regarding the quantification of NF-κB and M1 levels.

The M1 and M2 phenotypes of macrophages differently influence the outcome of muscular dystrophy [22]. While M1 macrophages are mainly related to myonecrosis, M2 macrophages are involved in muscle regeneration [23]. In agreement with our results regarding the M1 and M2 levels after LED therapy, it was recently reported that PBM modulates the inflammation phase, optimizing the transition from inflammation to regeneration in the tibialis anterior muscle subjected to cryolesion [8]. This study emphasizes that this transition improves tissue repair.

In our experimental conditions, concomitant with the transition from M1 to M2 macrophage phenotype, we also observed an improvement in dystrophic muscular damage. LED therapy led to a reduction in biochemical and histomorphological assessments of muscle fiber degeneration. LED therapy was able to reduce increments in CK levels in serum and increase CK content in muscle. In addition, LED treatment reduced skeletal muscle damage, as indicated by the decrease in IgG-positive fibers, corroborating with biochemical analyses. In agreement with these findings, similar effects of LED treatment were also reported in an experimental poisoning model (24). Furthermore, we evaluated the fibrotic area. Although the presence of M2 macrophages may be relevant for muscle regeneration in dystrophic muscle, it is important to consider that in the long term, this macrophage phenotype can lead to fibrosis [25] Thus, it is important to highlight that under our experimental conditions, although LED therapy increased M2 macrophage levels, it also promoted a reduction in the fibrotic area. In agreement with our results, PBM was observed to have a positive effect on the inflammatory process and on collagen organization and distribution in the repair process of rat skeletal muscle [26].

It is also important to highlight that LED therapy, by protecting dystrophic muscle from degeneration, led to a smaller number of regenerated muscle fibers. Another interesting finding related to the potential effects of LED therapy on muscle regeneration is the modulation of myogenic factors, such as MyoD and myogenin. In agreement with previous studies [14, 27], we observed that LED therapy accelerates muscle repair in dystrophic muscle, promoting a down-regulation of MyoD levels and an up-regulation of myogenin levels. The up-regulation of myogenin is particularly important, as myogenin is an essential regulator of adult myofiber growth and muscle stem cell homeostasis [28]. In addition, our experiments demonstrated that LED therapy led to an increase in MyHC-slow levels (which are more resistant to dystrophic pathology) [29] with a concomitant reduction in MyHC-fast levels. It was recently reported that increased MEK1-ERK1/2 signalling induces skeletal muscle slow fiber-type and reduces muscular dystrophy disease severity [30]. The MEK-ERK signalling pathway is also required for M2 macrophage phenotype polarization by promoting peroxisome proliferator-activated receptor-γ (PPARγ)-induced retinoic acid signalling [31]. Based on this, it is possible that the MEK-ERK pathway is related to the up-regulation of the M2 macrophage phenotype and slow muscle fibers observed in our experiments after LED therapy. Reinforcing this hypothesis, a previous study showed that PBM therapy enhances neural differentiation of dental Pulp stem cells via activation of the ERK1/2 signalling pathway [32].

The beneficial effects of LED therapy on muscle regeneration and the inflammatory process in dystrophic muscle can also justify our findings regarding the enhancement of behavioral activity (open field) and muscle function (grip strength and four limb hanging test). In addition, the reduction in the inflammatory process may be implicated in the decrease in ROS production. In the present study, LED therapy significantly reduced lipid peroxidation (4-HNE; autofluorescent lipofuscin granules) and ROS (reactive DHE area) production in dystrophic muscle.

These results align with previous work that demonstrates that PBM prevents oxidative stress in muscle injury animal models [33]. Furthermore, similar to previous studies [27, 34], we also observed that LED therapy promotes the reduction of NF-κB levels concurrently with the decrease in oxidative stress markers.

The decrease in oxidative stress and the inflammatory process after LED therapy may also be linked to the reduction of intracellular calcium concentration. One important consequence of increased intracellular calcium concentration is proposed to be enhanced production of ROS, which can cause muscle damage through direct effects on muscle fiber proteins and the membrane, as well as through the activation of inflammatory pathways [35]. In the present study, an increase in the levels of calsequestrin and Serca 1 was observed after LED therapy. These are important findings, as it has been reported that calsequestrin content and Serca determine normal and maximal Ca^{2+} storage levels in the sarcoplasmic reticulum of fast- and slow-twitch rat fibers [36]. In addition, Serca 1 overexpression minimizes skeletal muscle damage in dystrophic mouse models [37] and high levels of calsequestrin were found in the spared muscle of mdx mice [38]. Our results with calsequestrin and Serca1 suggest that modulation of calcium signalling pathways may also be one of the mechanisms by which LED therapy exhibits antioxidant and anti-inflammatory effects in dystrophic muscle.

In summary, the striking finding of this work is that LED therapy shifted the macrophage phenotype from M1 to M2 in treadmill-trained mdx mice, thereby enhancing tissue repair and mitigating the dystrophic phenotype. Our data also suggest that the beneficial effects of LED therapy in dystrophic muscle correlate with the interplay between calcium, oxidative stress and inflammation signalling pathways.

Acknowledgements This research was funded by Fundação de Amparo à Pesquisa do Estado de São Paulo (FAPESP; #2020/09733-4), Coordenação de Pessoal de Nível Superior-Brasil (CAPES) – Finance Code 001, CNPq and FAEPEX. V.A.P., H.N.M.S. and E.M. (#140845/2020-8; #130448/2022-2; #303471/2022-0; respectively) are the recipients of a CNPq fellowship. We thank Mrs. Deirdre Jane Donovan Giraldo for the English revision of the manuscript.

Author contributions V.A.P. conducted the study. V.A.P., H.N.M.S and E.M.F. contributed substantially to the acquisition of data, analysis and interpretation of data. E.M. and V.A.P. participated in the design of the study, were responsible for the management of the grant and coordination. E.M. and V.A.P. helped to draft the manuscript. All authors revised it critically for important intellectual content and gave final approval of the version to be submitted.

Data availability UNICAMP Research Data Repository (https://doi.org/10.25824/redu/MKWQGK).

Declarations

Conflict of interest All the authors declare that they do not have any conflict of interest.

References

1. Emery, A. E. H. (2002). The muscular dystrophies. *The Lancet, 359*(9307), 687–695. https://doi.org/10.1016/s0140-6736(02)07815-7
2. Shin, J., Tajrishi, M. M., Ogura, Y., & Kumar, A. (2013). Wasting mechanisms in muscular dystrophy. *The International Journal of Biochemistry & Cell Biology, 45*(10), 2266–2279. https://doi.org/10.1016/j.biocel.2013.05.001
3. Tidball, J. G., Welc, S. S., & Wehling-Henricks, M. (2018). Immunobiology of inherited muscular dystrophies. *Comprehensive Physiology, 8*(4), 1313–1356. https://doi.org/10.1002/cphy.c170052
4. Verhaart, I. E. C., & Aartsma-Rus, A. (2019). Therapeutic developments for Duchenne muscular dystrophy. *Nature Reviews. Neurology, 15*(7), 373–386. https://doi.org/10.1038/s41582-019-0203-3
5. Theret, M., Saclier, M., Messina, G., & Rossi, F. M. V. (2022). Macrophages in skeletal muscle dystrophies, an entangled partner. *Journal of Neuromuscular Diseases, 9*(1), 1–23. https://doi.org/10.3233/jnd-210737
6. Dadgar, S., Wang, Z., Johnston, H., Kesari, A., Nagaraju, K., Chen, Y.-W., Hill, D. A., Partridge, T. A., Giri, M., Freishtat, R. J., Nazarian, J., Xuan, J., Wang, Y., & Hoffman, E. P. (2014). Asynchronous remodeling is a driver of failed regeneration in Duchenne muscular dystrophy. *The Journal of Cell Biology, 207*(1), 139–158. https://doi.org/10.1083/jcb.201402079
7. Saclier, M., Ben Larbi, S., My Ly, H., Moulin, E., Mounier, R., Chazaud, B., & Juban, G. (2021). Interplay between myofibers and pro-inflammatory macrophages controls muscle damage in *mdx* mice. *Journal of Cell Science*. https://doi.org/10.1242/jcs.258429
8. Souza, N. H. C., Mesquita-Ferrari, R. A., Rodrigues, M. F. S. D., da Silva, D. F. T., Ribeiro, B. G., Alves, A. N., Garcia, M. P., Nunes, F. D., da Silva Junior, E. M., França, C. M., Bussadori, S. K., & Fernandes, K. P. S. (2018). Photobiomodulation and different macrophages phenotypes during muscle tissue repair. *Journal of Cellular and Molecular Medicine, 22*(10), 4922–4934. https://doi.org/10.1111/jcmm.13757
9. Hamblin, M. R. (2023). Photobiomodulation therapy for muscular dystrophy: Time for a trial? *Photobiomodulation, Photomedicine, and Laser Surgery, 41*(6), 245–247. https://doi.org/10.1089/photob.2023.0057
10. Silva, A. A. O., Leal-Junior, E. C. P., D'Avila, K. A. L., Serra, A. J., Albertini, R., França, C. M., Nishida, J. A., & de Carvalho, P. T. C. (2015). Pre-exercise low-level laser therapy improves performance and levels of oxidative stress markers in mdx mice subjected to muscle fatigue by high-intensity exercise. *Lasers in Medical Science, 30*(6), 1719–1727. https://doi.org/10.1007/s10103-015-1777-7
11. Macedo, A. B., Mizobuti, D. S., Hermes, T. A., Mâncio, R. D., Pertille, A., Kido, L. A., Cagnon, V. H. A., & Minatel, E. (2020). Photobiomodulation therapy for attenuating the dystrophic phenotype of M*dx* mice. *Photochemistry and Photobiology, 96*(1), 200–207. https://doi.org/10.1111/php.13179
12. De Luca, A. (2019). *Use of treadmill and wheel exercise for impact on mdx mice phenotype*. Treat-nmd.org. https://www.treat-nmd.org/wp-content/uploads/2023/07/MDX-DMD_M.2.1.001.pdf. Retrieved 10 Jan 2022.

13. Silva, H. N. M., Covatti, C., Rocha, G. L., Mizobuti, D. S., Mâncio, R. D., Hermes, T. A., Kido, L. A., Cagnon, V. H. A., Pereira, E. C. L., & Minatel, E. (2021). Oxidative stress, inflammation, and activators of mitochondrial biogenesis: Tempol targets in the diaphragm muscle of exercise trained-mdx mice. *Frontiers in Physiology, 12*, 649793. https://doi.org/10.3389/fphys.2021.649793
14. da Silva, H. N. M., Fernandes, E. M., Pereira, V. A., Mizobuti, D. S., Covatti, C., da Rocha, G. L., & Minatel, E. (2024). LEDT and Idebenone treatment modulate autophagy and improve regenerative capacity in the dystrophic muscle through an AMPK-pathway. *PLoS ONE, 19*(3), e0300006. https://doi.org/10.1371/journal.pone.0300006
15. Aartsma-Rus, A., & van Putten, M. (2014). Assessing functional performance in the mdx mouse model. *Journal of Visualized Experiments, 85*, e51303. https://doi.org/10.3791/51303
16. Carlson, C. G., Rutter, J., Bledsoe, C., Singh, R., Hoff, H., Bruemmer, K., Sesti, J., Gatti, F., Berge, J., & McCarthy, L. (2010). A simple protocol for assessing inter-trial and inter-examiner reliability for two noninvasive measures of limb muscle strength. *Journal of Neuroscience Methods, 186*(2), 226–230. https://doi.org/10.1016/j.jneumeth.2009.11.006
17. Manning, J., Kulbida, R., Rai, P., Jensen, L., Bouma, J., Singh, S. P., O'Malley, D., & Yilmazer-Hanke, D. (2014). Amitriptyline is efficacious in ameliorating muscle inflammation and depressive symptoms in the *mdx* mouse model of Duchenne muscular dystrophy. *Experimental Physiology, 99*(10), 1370–1386. https://doi.org/10.1113/expphysiol.2014.079475
18. De Luca, A., Pierno, S., Liantonio, A., Cetrone, M., Camerino, C., Fraysse, B., Mirabella, M., Servidei, S., Rüegg, U. T., & Conte Camerino, D. (2003). Enhanced dystrophic progression in mdx mice by exercise and beneficial effects of taurine and insulin-like growth factor-1. *The Journal of Pharmacology and Experimental Therapeutics, 304*(1), 453–463. https://doi.org/10.1124/jpet.102.041343
19. Sui, A., Chen, X., Demetriades, A. M., Shen, J., Cai, Y., Yao, Y., Yao, Y., Zhu, Y., Shen, X., & Xie, B. (2020). Inhibiting NF-κB signaling activation reduces retinal neovascularization by promoting a polarization shift in macrophages. *Investigative Ophthalmology & Visual Science, 61*(6), 4. https://doi.org/10.1167/iovs.61.6.4
20. Camille, N., & Dealtry, G. (2018). Regulation of M1/M2 macrophage polarization by Sutherlandia frutescens via NFkB and MAPK signaling pathways. *Suid-Afrikaanse Tydskrif Vir Plantkunde [South African Journal of Botany], 116*, 42–51. https://doi.org/10.1016/j.sajb.2018.02.400
21. Wu, X., Wang, Z., Shi, J., Yu, X., Li, C., Liu, J., Zhang, F., Chen, H., & Zheng, W. (2022). Macrophage polarization toward M1 phenotype through NF-κB signaling in patients with Behçet's disease. *Arthritis Research & Therapy*. https://doi.org/10.1186/s13075-022-02938-z
22. Villalta, S. A., Nguyen, H. X., Deng, B., Gotoh, T., & Tidball, J. G. (2008). Shifts in macrophage phenotypes and macrophage competition for arginine metabolism affect the severity of muscle pathology in muscular dystrophy. *Human Molecular Genetics, 18*(3), 482–496. https://doi.org/10.1093/hmg/ddn376
23. Mantovani, A., Sica, A., Sozzani, S., Allavena, P., Vecchi, A., & Locati, M. (2004). The chemokine system in diverse forms of macrophage activation and polarization. *Trends in Immunology, 25*(12), 677–686. https://doi.org/10.1016/j.it.2004.09.015
24. Campos, G. R. S., de Moura, K. M. B., Barbosa, A. M., Zamuner, L. F., Nadur-Andrade, N., Dale, C. S., Gutiérrez, J. M., Chavantes, M. C., & Zamuner, S. R. (2018). Light emitting diode (LED) therapy reduces local pathological changes induced by Bothrops asper snake venom. *Toxicon: Official Journal of the International Society on Toxinology, 152*, 95–102. https://doi.org/10.1016/j.toxicon.2018.07.029
25. Wehling-Henricks, M., Jordan, M. C., Gotoh, T., Grody, W. W., Roos, K. P., & Tidball, J. G. (2010). Arginine metabolism by macrophages promotes cardiac and muscle fibrosis in mdx muscular dystrophy. *PLoS ONE, 5*(5), e10763. https://doi.org/10.1371/journal.pone.0010763
26. Alves, A. N., Fernandes, K. P. S., Melo, C. A. V., Yamaguchi, R. Y., França, C. M., Teixeira, D. F., Bussadori, S. K., Nunes, F. D., & Mesquita-Ferrari, R. A. (2014). Modulating effect of low level-laser therapy on fibrosis in the repair process of the tibialis anterior muscle in rats. *Lasers in Medical Science, 29*(2), 813–821. https://doi.org/10.1007/s10103-013-1428-9
27. da Rocha, G. L., Mizobuti, D. S., da Silva, H. N. M., Covatti, C., de Lourenço, C. C., Salvador, M. J., Pereira, E. C. L., & Minatel, E. (2022). Multiple LEDT wavelengths modulate the Akt signaling pathways and attenuate pathological events in mdx dystrophic muscle cells. *Photochemical & Photobiological Sciences: Official Journal of the European Photochemistry Association and the European Society for Photobiology, 21*(7), 1257–1272. https://doi.org/10.1007/s43630-022-00216-0
28. Ganassi, M., Badodi, S., Wanders, K., Zammit, P. S., & Hughes, S. M. (2020). Myogenin is an essential regulator of adult myofibre growth and muscle stem cell homeostasis. *eLife, 9*, e60445. https://doi.org/10.7554/elife.60445
29. Webster, C., Silberstein, L., Hays, A. P., & Blau, H. M. (1988). Fast muscle fibers are preferentially affected in Duchenne muscular dystrophy. *Cell, 52*(4), 503–513. https://doi.org/10.1016/0092-8674(88)90463-1
30. Boyer, J. G., Prasad, V., Song, T., Lee, D., Fu, X., Grimes, K. M., Sargent, M. A., Sadayappan, S., & Molkentin, J. D. (2019). ERK1/2 signaling induces skeletal muscle slow fiber-type switching and reduces muscular dystrophy disease severity. *JCI Insight, 4*(10), e127356. https://doi.org/10.1172/jci.insight.127356
31. He, L., Jhong, J.-H., Chen, Q., Huang, K.-Y., Strittmatter, K., Kreuzer, J., DeRan, M., Wu, X., Lee, T.-Y., Slavov, N., Haas, W., & Marneros, A. G. (2021). Global characterization of macrophage polarization mechanisms and identification of M2-type polarization inhibitors. *Cell Reports, 37*(5), 109955. https://doi.org/10.1016/j.celrep.2021.109955
32. Zhang, X., Li, H., Tang, L., Zhu, B., Yang, W., Li, M., & Zhao, Y. (2024). Photobiomodulation therapy enhances neural differentiation of dental pulp stem cells via ERK1/2 signaling pathway. *Photochemistry and Photobiology, 100*(3), 646–655. https://doi.org/10.1111/php.13864
33. dos Santos, S. A., Serra, A. J., Stancker, T. G., Simões, M. C. B., dos Santos Vieira, M. A., Leal-Junior, E. C., Prokic, M., Vasconsuelo, A., Santos, S. S., & de Carvalho, P. T. C. (2017). Effects of photobiomodulation therapy on oxidative stress in muscle injury animal models: A systematic review. *Oxidative Medicine and Cellular Longevity, 2017*, 1–8. https://doi.org/10.1155/2017/5273403
34. da Rocha, G. L., Guimarães, D. S. P. S. F., da Cruz, M. V., Mizobuti, D. S., da Silva, H. N. M., Pereira, E. C. L., Silveira, L. R., & Minatel, E. (2024). Antioxidant effects of LEDT in dystrophic muscle cells: Involvement of PGC-1α and UCP-3 pathways. *Photochemical & Photobiological Sciences: Official Journal of the European Photochemistry Association and the European Society for Photobiology, 23*(1), 107–118. https://doi.org/10.1007/s43630-023-00506-1
35. Whitehead, N. P., Yeung, E. W., & Allen, D. G. (2006). Muscle damage in *mdx* (dystrophic) mice: role of calcium and reactive oxygen species. *Clinical and Experimental Pharmacology & Physiology, 33*(7), 657–662. https://doi.org/10.1111/j.1440-1681.2006.04394.x
36. Murphy, R. M., Larkins, N. T., Mollica, J. P., Beard, N. A., & Lamb, G. D. (2009). Calsequestrin content and SERCA determine normal and maximal Ca^{2+} storage levels in sarcoplasmic reticulum of fast- and slow-twitch fibres of rat. *The Journal of*

Physiology, 587(2), 443–460. https://doi.org/10.1113/jphysiol.2008.163162

37. Mázala, D. A. G., Pratt, S. J. P., Chen, D., Molkentin, J. D., Lovering, R. M., & Chin, E. R. (2015). SERCA1 overexpression minimizes skeletal muscle damage in dystrophic mouse models. *American Journal of Physiology. Cell Physiology, 308*(9), C699–C709. https://doi.org/10.1152/ajpcell.00341.2014
38. Pertille, A., De Carvalho, C. L. T., Matsumura, C. Y., Neto, H. S., & Marques, M. J. (2010). Calcium-binding proteins in skeletal muscles of the mdx mice: Potential role in the pathogenesis of Duchenne muscular dystrophy. *International Journal of Experimental Pathology, 91*(1), 63–71. https://doi.org/10.1111/j.1365-2613.2009.00688.x